



1 **Stratosphere-troposphere separation of nitrogen dioxide**
2 **columns from the TEMPO geostationary satellite**
3 **instrument**

4
5 **Jeffrey A. Geddes^{1,2}, Randall V. Martin^{1,3}, Eric J. Bucsela⁴, Chris A. McLinden⁵,**
6 **and Daniel J.M. Cunningham¹**

7 ¹Department of Physics and Atmospheric Science, Dalhousie University, Halifax, NS, Canada

8 ²Now at the Department of Earth and Environment, Boston University, Boston, MA, USA

9 ³Harvard-Smithsonian Center for Astrophysics, Cambridge, Massachusetts, USA

10 ⁴SRI International, Menlo Park, California, USA

11 ⁵Air Quality Research Division, Environment and Climate Change Canada, Toronto, ON,
12 Canada

13 *Correspondence to:* J.A. Geddes (jgeddes@bu.edu)

14

15 **Abstract**

16 Separating the stratospheric and tropospheric contributions in satellite retrievals of
17 atmospheric NO₂ column abundance is a crucial step in the interpretation and application of
18 the satellite observations. A variety of stratosphere-troposphere separation algorithms have
19 been developed for sun-synchronous instruments in low Earth orbit (LEO) that benefit from
20 global coverage, including broad clean regions with negligible tropospheric NO₂ compared to
21 stratospheric NO₂. These global sun-synchronous algorithms need to be evaluated and refined
22 for forthcoming geostationary instruments focused on continental regions, which lack this
23 global context and require hourly estimates of the stratospheric column. Here we develop and
24 assess a spatial filtering algorithm for the upcoming TEMPO geostationary instrument that
25 will target North America. Developments include using independent satellite observations to
26 identify likely locations of tropospheric enhancements, using independent LEO observations
27 for spatial context, consideration of diurnally-varying partial fields of regard, and a filter
28 based on stratospheric to tropospheric air mass factor ratios. We test the algorithm with LEO



1 observations from the OMI instrument with an afternoon overpass, and from the GOME-2
2 instrument with a morning overpass.

3 We compare our TEMPO field of regard algorithm against an identical global algorithm
4 to investigate the penalty resulting from the limited spatial coverage in geostationary orbit,
5 and find excellent agreement in the estimated mean daily tropospheric NO₂ column densities
6 ($R^2 = 0.999$, slope = 1.009 for July and $R^2 = 0.998$, slope = 0.999 for January). The algorithm
7 performs well even when only small parts of the continent are observed by TEMPO. The
8 algorithm is challenged the most by east coast morning retrievals in the wintertime (e.g. $R^2 =$
9 0.995 , slope = 1.038 at 1400 UTC). We find independent global low Earth observations
10 (corrected for time of day) provide important context near the field-of-regard edges. We also
11 test the performance of the TEMPO algorithm without these supporting global observations.
12 Most of the continent is unaffected ($R^2 = 0.924$ and slope = 0.973 for July and $R^2 = 0.996$ and
13 slope = 1.008 for January), with 90% of the pixels having differences of less than $\pm 0.2 \times 10^{15}$
14 molecules cm⁻² between the TEMPO tropospheric NO₂ column density and the global
15 algorithm. For near-real-time retrieval, even a climatological estimate of the stratospheric
16 NO₂ surrounding the field of regard would improve this agreement. In general, the additional
17 penalty of a limited field of regard from TEMPO introduces no more error than normally
18 expected in most global stratosphere-troposphere separation algorithms. Overall, we conclude
19 that hourly near-real-time stratosphere-troposphere separation for the retrieval of NO₂
20 tropospheric column densities by the TEMPO geostationary instrument is both feasible and
21 robust, regardless of the diurnally-varying limited field of regard.

22

23 **1 Introduction**

24 Nitrogen dioxide (NO₂) and nitrogen oxides in general are central to atmospheric
25 chemistry in both the troposphere and stratosphere (Finlayson-Pitts and Pitts, 1999; Seinfeld
26 and Pandis, 2016). In the stratosphere, nitrogen oxides are a key player in ozone (O₃)
27 depletion chemistry. In the troposphere, photolysis of NO₂ is responsible for the production of
28 O₃ whose buildup is associated with negative human health, ecosystem, and radiative forcing
29 impacts. Emissions of nitrogen oxides are also linked to the production of secondary
30 inorganic aerosol with impacts on both health and global climate. Observations of NO₂ in the
31 atmosphere are therefore critical given its roles in air quality and atmospheric chemistry.



1 Satellite remote sensing of NO₂ from instruments in low Earth orbit has offered
2 extraordinary insight into global nitrogen oxide processes. Among many applications,
3 observations from GOME (1996-2003), SCIAMACHY (2002-2011), OMI (2004-), and
4 GOME-2 (2007-) have contributed to understanding global and regional patterns in nitrogen
5 oxide emissions (e.g. Beirle et al. 2003; Duncan et al. 2013; Jaegle et al., 2005; Konovalov et
6 al., 2008; Lamsal et al., 2011; Martin et al., 2003; Miyazaki et al., 2016; Richter et al. 2005;
7 Russell et al. 2012), evaluating ground-level air quality in the absence of traditional
8 monitoring data (e.g. Bechle et al., 2013; Boersma et al. 2009; Geddes et al., 2016; Lamsal et
9 al. 2008; McLinden et al., 2012), and constraining nitrogen oxide deposition out of the
10 atmosphere (e.g. Geddes and Martin, 2017; Jia et al., 2016; Nowlan et al., 2014). A key step
11 in these applications is the separation of stratospheric and tropospheric NO₂ from the total
12 column derived from the satellite observation, a process that can introduce substantial
13 uncertainty the final tropospheric column estimates (Beirle et al. 2016; Boersma et al., 2004;
14 Bucsela et al. 2013; Martin et al., 2002).

15 Separating the stratospheric and tropospheric contributions to the total column has been
16 performed using a number of approaches, varying in complexity and in the assumptions that
17 are made. The simplest approach is the Pacific reference sector method (Beirle et al., 2003;
18 Martin et al., 2002; Richter and Burrows, 2002) in which stratospheric NO₂ is treated as
19 longitudinally homogeneous so that stratospheric NO₂ in any location can be estimated by
20 using the measured NO₂ over the remote Pacific at the same latitude. Tropospheric NO₂ in the
21 reference sector might either be ignored altogether (e.g. Richter and Burrows, 2002) or
22 accounted for using a model estimate (e.g. Martin et al., 2002). While the treatment of zonal
23 invariance is reasonable for low- to mid-latitudes, stratospheric dynamics (especially in the
24 vicinity of polar vortices) raise concerns at higher latitudes of relevance for planned
25 geostationary missions.

26 Image processing and spatial filtering techniques are an extension of the reference sector
27 method (Bucsela et al., 2006, 2013; Leue et al., 2001; Valks et al., 2011; Velders et al., 2001;
28 Wenig et al., 2004), whereby stratospheric NO₂ is estimated by interpolating between regions
29 that are classified as having negligible tropospheric NO₂. This might be accomplished for
30 example by using only cloudy scenes over the oceans (e.g. Leue et al., 2001), or by applying a
31 pollution “mask” given prior estimates of tropospheric NO₂ (e.g. Bucsela et al., 2006; Valks
32 et al., 2011). Bucsela et al. (2013) proposed a masking scheme that combines a prior estimate



1 of tropospheric NO₂ with radiative transfer calculations to allow polluted pixels to remain if
2 the scene is cloudy (obscuring lower tropospheric NO₂), and exclude unpolluted regions
3 where tropospheric NO₂ signal may still be significant due to high tropospheric air mass
4 factors. An elegant variation of this spatial filtering approach is the STRatospheric Estimation
5 Algorithm from Mainz (STREAM), developed by Beirle et al. (2016). Instead of binary
6 masks based on arbitrary thresholds, STREAM applies a weighted convolution scheme where
7 cloudy observations are given a high weight and polluted observations (based on a prior
8 estimate) are given low weight. These spatial filtering approaches developed exclusively for
9 global observational coverage from low Earth orbit offer valuable guidance on the
10 development of geostationary stratosphere-troposphere separation algorithms.

11 Nadir observations are also used in assimilation approaches where model predictions of
12 the stratospheric NO₂ column density are adjusted towards the observed column density. For
13 example, stratosphere-troposphere separation in the Dutch NO₂ algorithm is achieved by
14 assimilating observed NO₂ columns with model NO₂ column predictions from the TM4
15 chemical transport model forced by ECMWF meteorological data (Boersma et al., 2007;
16 Dirksen et al., 2011). In that approach, modeled NO₂ profiles are convolved into line-of-sight
17 (“slant”) columns using averaging kernels, and the difference between modeled and observed
18 slant column densities are used to force the modeled columns to an “analysed” state. Using
19 the most recent observations available, the “analysed” state can be used in a forecast model
20 run to predict the stratospheric field for near-real time retrievals (Boersma et al. 2007).

21 In some cases, independent stratospheric observations may be used in the separation of
22 stratospheric and tropospheric NO₂. For example, the SCIAMACHY instrument made almost
23 coincident nadir and limb measurements (Bovensmann et al., 1999) and this matching was
24 exploited in algorithms by Beirle et al. (2010) and Hilboll et al. (2013). Even non-coincident
25 limb-nadir matching has been exploited for stratosphere-troposphere separation, as in the case
26 of OSIRIS and OMI (Adams et al., 2016). Sussmann et al. (2005) demonstrate how
27 simultaneous ground-based measurements (especially at mountain sites) could be applied for
28 stratosphere-troposphere separation algorithm validation.

29 To date, all of the above approaches to stratosphere-troposphere separation have been
30 developed using the large coverage of observations provided by instruments in low Earth
31 orbit. Questions remain about how well the separation can be performed without the global
32 context and where clean tropospheric background signals are limited. Stratosphere-



1 troposphere separation algorithms need to be evaluated and refined for the restricted field of
2 regard of future geostationary instruments such as TEMPO (Zoogman et al., 2017), Sentinel-4
3 (Veihelmann et al. 2015), and GEMS (Lasnik et al. 2014).

4 TEMPO (“Tropospheric Emissions: Monitoring of Pollution”), launching between 2019-
5 2021, will provide space-based measurements in geostationary orbit with a field of regard
6 over North America from southern Canada to Mexico City and the Bahamas (Zoogman et al.,
7 2017). The spectrometer has spectral ranges of 290-490 nm (at 0.57 nm resolution) and 540-
8 740 nm (at 0.2 nm resolution), allowing retrieval of tropospheric composition with fine spatial
9 resolution (up to 2.1 km North-South x 4.4 km East-West instantaneous field of view).
10 Scanning occurs from east to west, with hourly revisits. Among its standard products
11 available at roughly 4 km x 8 km spatial resolution will be hourly NO₂ column abundance.
12 Here, we develop a standard stratosphere-troposphere separation algorithm for the
13 observations of NO₂ from TEMPO, and examine in detail the potential information penalty
14 associated with the limited TEMPO field of regard compared to an identical global algorithm.

15

16 **2 Satellite Observations**

17 To develop and test our algorithm, we use data from two low Earth orbiting instruments,
18 with afternoon and morning overpasses. We use NO₂ column densities derived from OMI on
19 board the Aura satellite launched in 2004. OMI is a nadir-viewing spectrometer in low Earth
20 orbit crossing the equator around 13:30 local time, with a variable horizontal resolution of 13
21 km x 24 km at nadir. Line-of-sight (“slant”) columns are retrieved from spectral fitting of
22 back-scattered and reflected solar radiation within the 405-465 nm wavelength range, and
23 corrected for instrumental artifacts (Bucsela et al., 2013). We use the Version 2.1 Collection 3
24 data product from NASA (Krotkov et al. 2017, publicly available at
25 http://disc.sci.gsfc.nasa.gov/Aura/data-holdings/OMI/omno2_v003.shtml), including
26 stratospheric and tropospheric air mass factors provided with the data to relate slant and
27 vertical columns (Bucsela et al., 2013). We use the artifact-corrected slant column densities
28 (“destriping”) and the tropospheric and stratospheric air mass factors calculated for each
29 pixel. All data are first gridded to a 0.1° x 0.1° regular grid.

30 We also make use of NO₂ column densities derived from GOME-2, on board the MetOp-
31 A satellite launched in 2006. GOME-2 is another nadir-viewing spectrometer in low Earth
32 orbit, crossing the equator around 09:30 local time with a constant horizontal resolution of 80



1 km x 40 km in its default swath. Spectral fitting is performed within the 420-450 nm
2 wavelength range. Here we use the TM4NO2A retrieval (Boersma et al. 2004) version 2.3
3 data product from KNMI (available from <http://www.temis.nl/airpollution/no2.html>) along
4 with the included air mass factors.

5 We restrict all data to solar zenith angles smaller than 80°.

6

7 **3 Estimating Stratospheric NO₂ over the TEMPO Field of Regard**

8 Here we describe our approach to estimate the stratospheric NO₂ column in TEMPO
9 observations. As a foundation for our method, we begin with the approach used in the current
10 operational algorithm for OMI (Bucsela et al., 2013). This algorithm has demonstrated high
11 quality performance against validation data sets (Ialongo et al., 2016; Lamsal et al., 2014;
12 Bucsela et al., 2013), is computationally fast, and is suitable for near-real-time retrievals. Our
13 own implementation of this algorithm reproduces the operational global stratospheric NO₂
14 product well ($r = 0.99$ and a slope of 1.01). As described below, we build on this algorithm for
15 TEMPO by modifying certain smoothing/filtering steps, using a satellite-derived prior
16 estimate of tropospheric NO₂, incorporating observations surrounding the TEMPO field of
17 regard from independent low Earth orbit instruments, and by considering partial fields of
18 regard relevant to TEMPO.

19 Figure 1 shows the stepwise implementation of our TEMPO stratosphere-troposphere
20 separation algorithm for an example day in July. As a surrogate for TEMPO observations, we
21 begin by restricting the OMI total slant NO₂ column observations to the anticipated TEMPO
22 field of regard below a solar zenith angle threshold of 80° (Figure 1a). The expected coverage
23 of TEMPO extends from as far south as Mexico City, northward to include southern Canada
24 (covering as far north as the oil sands region in Alberta for example). The pattern along the
25 orbit tracks in Figure 1a results from the changing OMI viewing zenith angle (with higher
26 slant columns for larger viewing angles).

27 An initial estimate of the stratospheric vertical NO₂ column (V_{init}) can be obtained by:

$$28 \quad V_{init} = \frac{(S - S_{trop,prior})}{A_{strat}} \quad \text{Equation 1}$$

29 where S is the total slant column density, A_{strat} is the stratospheric air mass factor, and $S_{trop,prior}$
30 accounts for small contributions from the troposphere (Bucsela et al. 2013). Bucsela et al.



1 (2013) estimated the tropospheric contribution using model values. To provide a more
2 accurate constraint on tropospheric contributions, we use the monthly mean tropospheric NO₂
3 columns derived from independent GOME-2 observations as an initial a-priori tropospheric
4 NO₂ estimate. This concept enables the use of spatial information observed from satellite, and
5 could be readily adapted to use TROPOMI observations at finer resolution. The use of a
6 satellite-derived a-priori reduces the use of chemical transport model information in the
7 stratosphere-troposphere separation algorithm (although we revert to a model estimate if
8 quality controlled satellite coverage is not available, e.g. due to systematically high cloud
9 fractions). We transform this satellite-derived a priori tropospheric NO₂ vertical column
10 ($V_{trop,prior}$) into slant column space using the tropospheric air mass factors (A_{trop}) provided with
11 the OMI data:

$$12 \quad S_{trop,prior} = V_{trop,prior} \cdot A_{trop} \quad \text{Equation 2.}$$

13 Figure 1b shows our initial estimate of stratospheric vertical NO₂ columns over the TEMPO
14 domain resulting from the combination of Equation 1 and 2. We already see that this
15 stratospheric NO₂ estimate varies predominately as a function of latitude, although
16 anomalously low values are seen over some urban centers (e.g. around Los Angeles, Chicago,
17 and New York) where the a-priori tropospheric NO₂ slant column is large.

18 To exclude locations where this initial stratospheric vertical column estimate is likely
19 biased, we make use of the masking approach from Bucsel et al. (2013). This is based on
20 eliminating pixels where tropospheric contamination is high (or where the initial stratospheric
21 vertical column estimate would exceed the actual stratospheric vertical column by some
22 reasonable value) by requiring:

$$23 \quad \frac{S_{trop,prior}}{A_{strat}} < 0.3 \times 10^{15} \text{ cm}^{-2} \quad \text{Equation 3.}$$

24 On a typical day in July, this means that contamination from the troposphere would be less
25 than ~10% percent of the stratospheric NO₂ estimate (which generally ranges from 2-4 x 10¹⁵
26 cm⁻² over the TEMPO field of regard). Figure 1c shows the result of this masking step. The
27 threshold removes all the urban regions with anomalously low values in Figure 1b, in addition
28 to many other areas. Sensitivity tests show that the final stratospheric NO₂ estimate varies by
29 less than 5% for changes in this threshold between 0.2 x 10¹⁵ or 0.4 x 10¹⁵ cm⁻², consistent
30 with the generally small sensitivity found by Bucsel et al. (2013)). On this example day (and



1 for the month of July on average) the masking threshold of $0.3 \times 10^{15} \text{ cm}^{-2}$ removes 55% of
2 the original data within the TEMPO field of regard. We find coverage is best over Canada and
3 over the Pacific Ocean, with less coverage over the rest of the continent and the Atlantic
4 Ocean. The original global algorithm removes ~28% of the available global data on average
5 for days in July, since tropospheric NO_2 columns are generally lower elsewhere in the world.

6 Since $S_{trop,prior}$ is calculated based on radiative transfer calculations (A_{trop}) in addition to
7 the a priori tropospheric NO_2 vertical column (Equation 2), this masking approach in principle
8 allows for polluted pixels to remain if the lower tropospheric signal is sufficiently suppressed
9 by clouds resulting in a low tropospheric air mass factor (or conversely excludes pixels with a
10 considerable tropospheric signal due to high surface reflectivity). We investigated the use of
11 explicitly cloudy scenes (cloud radiance fraction > 0.9), which could suppress the signal from
12 below. Mid-level clouds (600-400 hPa) are the least likely to contain significant NO_x mixed
13 in from the surface, or lightning NO_x associated with higher clouds. We find that most
14 ($>75\%$) of the pixels that meet these criteria are already retained by our original masking
15 algorithm. Incorporating the remaining cloudy pixels to the masked data increases data
16 coverage by less than 1%. Given the uncertainties in retrieving cloud properties, uncertainties
17 in cloudy air mass factors, and the minimal added value of this dataset, we disregard adding
18 the remaining cloudy pixels to our algorithm.

19 In Bucseła et al. (2013), the remaining unmasked data are binned and un-filled bins are
20 interpolated using 2-dimensional averaging with a 30° longitude x 20° latitude moving
21 window. In our case, this step necessarily precludes information from outside the TEMPO
22 field of regard over the mostly pristine oceans from being used in the 2-D averaging. As we
23 will show, this leads to biases near the field of regard edges when compared to a global
24 algorithm, since the averaging window is disproportionately impacted by observations with
25 continental influence. We reduce this bias by incorporating independent global observations
26 from low Earth orbit that can provide context outside of the TEMPO field of regard. This
27 approach exploits the independent low Earth orbit observations that are expected throughout
28 the lifespan of TEMPO (e.g. GOME-2, TROPOMI).

29 Here, we employ GOME-2 observations as an independent dataset to estimate
30 stratospheric NO_2 at GOME-2 overpass time outside the TEMPO field of regard by using an
31 identical algorithm on this global data. We empirically transform the GOME-2 stratospheric
32 NO_2 estimate to the TEMPO observation time (here, the OMI overpass time), using the



1 climatological 30-day running mean local ratio of GOME-2 to OMI stratospheric NO₂. A
2 similar observational or model climatology could readily be constructed with TEMPO data
3 after launch based on the available low Earth orbit observations at the time. Figure 1d shows
4 the outcome of this approach. The GOME-2 observations outside of the TEMPO field of
5 regard retain the same magnitude and latitudinal gradient as the available observations within
6 the TEMPO field of regard, suggesting that the additional context from an independent low
7 Earth orbit instrument can be useful even when they are from a different time of day.
8 Before interpolating the unfilled bins, we apply a boxcar filter using a moving 15° x 10°
9 window as follows. First, our boxcar filter returns a smoothed array using the following
10 algorithm:

$$R_i = \frac{1}{w} \sum_{j=0}^{w-1} A_{i+j-w/2} \quad \text{where} \quad \frac{(w-1)}{2} \leq i \leq N - \frac{(w+1)}{2}$$

11 Equation 4

12 where w is the smoothing width (in our case, defined in two dimensions by both a length and
13 width), R_i is the i -th point in the smoothed data, and A_i is the i -th point in the original data. For
14 data points where the neighborhood includes points outside the array, the nearest edge points
15 are used to compute the smoothed result. The variance of the original data is also calculated
16 using a similar algorithm. Any value that lies outside of the moving window average by ± 1.5
17 standard deviations is removed. While the Bucsele et al. (2013) algorithm uses the same
18 window size in a boxcar filtering step, it is performed later and only remove values above the
19 mean (“hotspots”). Here, we perform this boxcar filter in both directions (above and below
20 the mean) to remove anomalously low values that might result from a biased a-priori
21 tropospheric estimate that was not accounted for in the masking step (avoiding negative
22 stratospheric NO₂ values being retained in subsequent steps), and to remove anomalously
23 high values that might result from transient pollution events that were likewise missed in the
24 masking step. We perform this boxcar filter twice to strictly remove outliers from regions
25 with noisy data.

26 Missing bins are then interpolated using a 30° longitude x 20° latitude moving window.
27 We tested smaller window sizes and found that they could introduce unphysical variability,
28 and/or leave missing data. Figure 1e shows how all the missing data over the TEMPO domain
29 are successfully filled using this window size. A few remaining “hot spots” are accounted for
30 in a third pass of the boxcar filter.



1 To obtain our final stratospheric NO₂ column estimate, we apply a final simple
2 smoothing step with a 5° x 3° window, as in Bucsele et al. (2013). The smaller box-car
3 window size in this step recognizes, and allows for, some regional scale variability in the
4 stratosphere. Figure 1f shows the final stratospheric NO₂ column estimate over the TEMPO
5 field of regard. Variation is primarily a function of latitude, from around 2 x 10¹⁵ molec cm⁻²
6 at the lowest latitudes in the field of regard (~20° latitude) to around 4 x 10¹⁵ molec cm⁻² at
7 the highest latitudes (~60° latitude). It is also apparent that this spatial filtering algorithm
8 allows for important regional scale variability to be retained in the stratospheric estimate.

9 Figure 2 shows the results of the same algorithm from an example day in January. The
10 shape of the expected TEMPO domain is impacted by large solar zenith angles at the highest
11 latitudes (we again use a solar zenith angle cut-off of 80°). Tropospheric enhancements
12 feature more prominently in the total slant column (Figure 2a) than in July since stratospheric
13 NO₂ columns are lower in the winter, and tropospheric NO₂ columns are higher. Figure 2b
14 shows the initial stratospheric estimate (V_{ini}) from Equation 1, again using the monthly mean
15 GOME-2 tropospheric NO₂ column as an a priori estimate (Equation 2). Figure 2c shows the
16 result of applying the masking threshold (Equation 3). We find this threshold removes 51% of
17 the available data on average for this month (~21% of the available data are removed in the
18 global algorithm in January). Over the TEMPO domain we find that a slightly smaller fraction
19 pixels are removed in January compared to July because, despite having generally higher NO₂
20 tropospheric column densities, tropospheric air mass factors across the northeast are
21 extremely low at this time of year (discussed below). The low values are primarily due to
22 increased wintertime cloudiness. In this case, the masking threshold did not remove a strong
23 enhancement over the center of the continent. This highlights some criticism by Beirle et al.
24 (2016) of spatial filtering algorithms that rely strongly on a-priori climatologies wherein
25 transient tropospheric events could be misinterpreted as stratospheric. We find that varying
26 the magnitude of the threshold (Equation 3) does not successfully correct for this, since our
27 masking approach is based on a monthly mean and does not identify transient events, but this
28 feature is diminished in subsequent steps. Figure 2d shows the estimated stratospheric NO₂
29 outside of the TEMPO field of regard from the independent GOME-2 observations. Again,
30 these low Earth orbit observations provide powerful context despite being from a different
31 time of day. Figure 2e shows the result of the first two passes of the boxcar filter, and
32 interpolating unfilled bins using the 30° longitude x 20° latitude moving window.



1 Figure 2f shows the final stratospheric NO₂ estimate after the final pass of the statistical
2 test and 5° x 3° smoothing. The large enhancement of NO₂ over the continent has been
3 substantially dampened by our statistical filtering. The variability in the stratospheric NO₂
4 column is again generally latitudinal as expected, with values above 2 x 10¹⁵ molec cm⁻²
5 at the low latitudes, and below 1 x 10¹⁵ molec cm⁻² at the high latitudes.

6 The full TEMPO domain will have simultaneous sunlit coverage from about 1400 UTC
7 to 2300 UTC in July, and for only a few hours in January, based on a solar zenith angle
8 threshold of ~80°. Of concern is the lack of coverage over the west coast in the morning, and
9 over the east coast in the evening, where sunlit observations will not be available. Under these
10 circumstances, the stratospheric separation algorithm is challenged by even narrower spatial
11 domains. We evaluate these cases by repeating the calculations at specific times of day.

12 Figure 3 shows how the TEMPO algorithm would operate for 1130 Coordinated
13 Universal Time (UTC), 6:30 a.m. Eastern Standard Time (EST), on the example day in July.
14 Daylight observations over eastern North America are available by this time, without
15 coverage over the rest of the continent. All the algorithm steps are identical to those in Figure
16 1 and Figure 2 other than treatment of this partial coverage (additional near-real-time
17 considerations are discussed in Section 5). Figure 3a shows the OMI total slant columns. By
18 6:30 a.m. EST TEMPO observes only eastern North America. The availability of observations
19 increases in width northward because of the TEMPO viewing geometry. Figures 3b and 3c
20 show the initial stratospheric estimate (according to Equation 1) and the masked stratospheric
21 estimate (according to Equation 3) respectively. Figure 3d shows the independent low Earth
22 orbit observations from GOME-2 outside of the TEMPO field of regard. The observations are
23 binned, pass the statistical filtering steps, and interpolated in Figure 3e. The final stratospheric
24 estimate is shown in Figure 3f. Comparing this final stratospheric NO₂ estimate with the
25 estimate in Figure 1f (where coverage over the whole continent is assumed to be available),
26 we see the reduced coverage has negligible impact the final stratospheric estimate, and
27 identical spatial features are preserved ($R^2 = 0.995$).

28 Likewise, Figure 4 shows how the algorithm would operate on the example day in
29 January at 2330 UTC, or 3:30 pm Pacific Standard Time (PST). In addition to the loss of
30 observations in the east due to the time of day, larger solar zenith angles in the north at this
31 time of year further diminish coverage. Again, the subsequent steps are otherwise identical to
32 those in Figures 1 through 3. Figure 4a shows the OMI total slant columns. Observations are



1 available over parts of the Pacific Northwest, with coverage widening southward so that
2 observations are available from California to the western edge of Texas, and over western
3 parts of Mexico. Figure 4b and 4c show the initial stratospheric estimate (according to
4 Equation 1) and the masked stratospheric estimate (according to Equation 3) respectively.
5 Figure 4d shows how the independent low Earth orbit observations from again GOME-2
6 provide coverage outside of the TEMPO field of regard. After binning and interpolation
7 (Figure 4e) followed by hot spot removal and smoothing, the final TEMPO stratospheric
8 estimate is shown in Figure 4f. Comparing this stratospheric NO₂ estimate with Figure 2f
9 (where coverage over the whole continent is assumed to be available) demonstrates again how
10 the reduced coverage has negligible impact the final stratospheric estimate, and identical
11 spatial features are preserved ($R^2 = 0.997$).

12 Next, we examine in detail the potential information penalty associated with the limited
13 TEMPO field of regard compared to a global algorithm, and demonstrate quantitatively that
14 our approach can produce a tropospheric NO₂ estimate that is consistent with a global
15 algorithm, regardless of the time of day.

16

17 **4 Stratosphere-Troposphere Separation over the TEMPO Field of Regard**

18 The final step in the algorithm is the subtraction of the stratospheric NO₂ estimate from
19 the total slant column to obtain the tropospheric NO₂ column by:

$$20 \quad V_{trop} = \frac{(S - V_{strat} \cdot A_{strat})}{A_{trop}} \quad \text{Equation 5}$$

21 For this calculation we use the stratospheric and tropospheric air mass factors provided with
22 the OMI data product (the operational TEMPO algorithm would use TEMPO air mass
23 factors).

24 The difference between two tropospheric NO₂ column retrievals ($V_{trop,2}$ and $V_{trop,1}$) that
25 result from two different stratospheric NO₂ estimates ($V_{strat,2}$ and $V_{strat,1}$), but identical slant
26 columns and air mass factors, is directly proportional to the ratio of the tropospheric to
27 stratospheric air mass factors:

28

$$29 \quad V_{trop,2} - V_{trop,1} = \frac{A_{strat}}{A_{trop}} (V_{strat,2} - V_{strat,1}) \quad \text{Equation 6}$$



1 This means that differences (or errors) in stratospheric NO₂ estimates are magnified in the
2 tropospheric NO₂ column depending on the local air mass factors. This issue is particularly
3 important over the eastern US in the winter, where tropospheric air mass factors can be very
4 low (<0.1), and stratospheric air mass factors can be high (~5) depending on viewing
5 geometry. Figure 5 shows the stratospheric and tropospheric air mass factors for January 15,
6 2007. Over areas of the eastern US, where clouds prevail, the tropospheric air mass factors are
7 exceedingly small (~0.01), which gives rise to extremely large A_{strat}/A_{trop} ratios (>200). In
8 other words, residuals between two stratospheric NO₂ algorithms can become magnified by
9 more than two orders of magnitude in the troposphere.

10 The impact of errors in the tropospheric column due to this issue can be minimized by
11 excluding observations with high stratospheric to tropospheric air mass factor ratios. This is
12 also based on the logic that such values indicate tropospheric NO₂ is making a small
13 contribution to the measured signal (and as a result, the tropospheric NO₂ retrieval should
14 have high uncertainty). For this reason, we restrict all tropospheric NO₂ estimates to where
15 the local stratospheric to tropospheric air mass factor ratios are less than 5.

16 Figure 6 shows the stratospheric and tropospheric NO₂ columns estimated for July 15,
17 2007. The top panels display the stratospheric and tropospheric NO₂ columns as derived from
18 our TEMPO algorithm that employs the OMI data as a surrogate for TEMPO observations,
19 with adjacent GOME-2 data provided context outside the field of regard. The middle panels
20 display the stratospheric and tropospheric columns derived from implementing our algorithm
21 globally with OMI data alone (the results are restricted to the TEMPO field of regard in the
22 figure to facilitate comparison). The bottom panel shows the differences between our TEMPO
23 algorithm and the global algorithm. We find excellent spatial agreement in the tropospheric
24 NO₂ estimate between the two algorithms ($R^2 = 0.997$, slope = 1.008). More than 95% of the
25 pixels have differences that are smaller than $\pm 0.1 \times 10^{15}$ molec cm⁻².

26 Figure 7 compares the stratospheric and tropospheric NO₂ column estimates from the
27 TEMPO and global algorithms for January 15, 2007. The loss of coverage in the troposphere
28 (mostly over the eastern US) is a result of the air mass factor issue discussed above, leading to
29 tropospheric NO₂ retrievals with low information content. The spatial agreement in the
30 tropospheric NO₂ estimates that remain is excellent across the domain ($R^2 = 0.996$ slope =
31 0.999). The magnitude of the differences in the stratospheric columns become larger in the



1 troposphere, exceeding 0.5×10^{15} molec cm^{-2} near the edges. Nonetheless, ~95% of the pixels
2 are consistent with the global version of the algorithm to within 0.25×10^{15} molec cm^{-2} .

3 Figure 8 shows the monthly mean tropospheric NO_2 columns resulting from our TEMPO
4 stratosphere-troposphere separation algorithm for both July and January, and the difference
5 versus results from the global algorithm. We find that our TEMPO algorithm produces
6 monthly mean results with negligible difference compared to the global algorithm, even at the
7 field of regard edges. The correlation between the two algorithms is excellent ($R^2 = 0.999$ and
8 slope = 1.009 for July, $R^2 = 0.998$ and slope = 0.999 for January). For July, more than 99% of
9 the pixels have differences that are smaller than $\pm 0.05 \times 10^{15}$ molec cm^{-2} . For January, more
10 than 90% of the pixels have differences that are smaller than $\pm 0.05 \times 10^{15}$ molec cm^{-2} , and
11 more than 99% of the pixels have differences that are smaller than $\pm 0.10 \times 10^{15}$ molec cm^{-2} . In
12 other words, our TEMPO-specific algorithm performs almost identically to the low Earth
13 orbit algorithm that uses all available global data. There are some random errors near the field
14 of regard edges on individual days (Figures 6 and 7), but these nearly disappear in the
15 monthly average (Figure 8)

16 Figure 9 shows the July monthly mean tropospheric NO_2 columns resulting from
17 retrievals at 1130 UTC (east coast summer morning) and at 0200 UTC (west coast summer
18 evening). The east coast morning retrieval example exhibits small positive biases over some
19 the Great Lakes region compared to the global algorithm, but overall the spatial agreement
20 remains excellent ($R^2 = 0.996$ and slope = 1.015). More than 90% of the pixels have
21 differences that are smaller than $\pm 0.05 \times 10^{15}$ molec cm^{-2} , and more than 98% of the pixels
22 have differences that are smaller than $\pm 0.10 \times 10^{15}$ molec cm^{-2} . The west coast summer
23 evening example also exhibits excellent performance overall ($R^2 = 0.998$ and slope = 0.994).
24 In this case, more than 98% of the pixels have differences that are smaller than $\pm 0.05 \times 10^{15}$
25 molec cm^{-2} .

26 Figure 10 shows the January monthly mean tropospheric NO_2 columns resulting from
27 retrievals at 1400 UTC (east coast winter morning) and 2330 UTC (west coast winter
28 evening). The bottom panels in Figure 10 show the difference between the results from our
29 TEMPO algorithm and the results from the global algorithm. In the east coast winter case,
30 spatial agreement is still very good in general ($R^2 = 0.995$), but we find noticeable
31 degradation in the absolute performance over the continent compared to the global algorithm
32 resulting from this partial field of view (slope = 1.038). The west coast winter evening



1 retrieval performs better overall ($R^2 = 0.999$, slope = 1.007). Although the algorithm performs
2 poorest in the east coast winter morning case, ~90% of the tropospheric pixels still have
3 differences that are less than 0.2×10^{15} molec cm⁻², a commonly accepted estimate of the
4 stratospheric uncertainty resulting from stratosphere-troposphere separation in NO₂ retrieval
5 algorithms (Boersma et al. 2004). Moreover, two hours later at 1600 UTC when the field of
6 regard has expanded across the Great Lakes region, into the middle of North America, and
7 covers most of Mexico, this issue disappears ($R^2 = 0.999$, slope = 0.998). In other words, as
8 spatial coverage expands, the absolute constraint on stratospheric NO₂ becomes more robust.

9 This highlights the challenge of accurate wintertime tropospheric NO₂ retrievals
10 (especially over eastern North America) when pollution is primarily in a shallow boundary
11 layer close to the surface where satellite remote sensing sensitivity is lowest. The partial
12 TEMPO field of regard in this case exacerbates the problem, but the challenge is not unique
13 to TEMPO retrievals.

14 Finally, we further test the performance of this algorithm at other times of day by
15 repeating the same steps as above, but using GOME-2 observations as a surrogate for
16 TEMPO. For this, we swap all instances of the OMI observations (overpass time ~ 13:30)
17 with GOME-2 observations (overpass time ~09:30), and vice versa. In other words, the
18 GOME-2 observations are restricted to the anticipated field of regard, and we use a monthly
19 from OMI as our a priori tropospheric column and the daily observations from OMI as
20 supporting global observations outside the TEMPO field of regard. We find the performance
21 at this morning overpass time is as good as the mid-afternoon overpass time ($R^2 = 0.999$,
22 slope = 1.005 for July; and $R^2 = 0.999$, slope = 1.005 for January), providing more evidence
23 that our approach works equally well at different times of day.

24

25 **5 Near-Real-Time Considerations**

26 For retrievals in near-real time (i.e. within an hour of the observation), independent
27 global observations in low Earth orbit may not be available (e.g. unexpected issues with low
28 Earth orbit observation processing). Here we test the performance of the TEMPO algorithm
29 without the supporting global observations by carrying out the identical steps outlined in
30 Sections 3 and 4 except without incorporating the GOME-2 observations outside the TEMPO
31 field of regard. Comparing these results with the global algorithm isolates the penalty due to



1 the limited TEMPO spatial domain alone, since the steps are otherwise computationally
2 identical.

3 Figure 11 shows the mean July and January tropospheric columns resulting from this
4 near-real time test. The spatial correlation with the global algorithm is still strong overall (R^2
5 = 0.924 and slope = 0.973 for July and $R^2 = 0.996$ and slope = 1.008 for January), and
6 between 90-95% of pixels in both July and January differ from the global algorithm by less
7 than 0.2×10^{15} molec cm^{-2} . We find that, compared to a global algorithm, this stratosphere-
8 troposphere separation approach gives rise to noticeable systematic biases near the field of
9 regard edges (including Mexico, the Caribbean, and northern Canada). The differences are
10 due to the lack of supporting data outside of the TEMPO field of regard.

11 This is most evidently a problem near the northern/southern borders of the field of regard,
12 given the strong gradient in stratospheric NO_2 as a function of latitude. At low latitudes, when
13 the averaging windows intersect with the field of regard, the global algorithm would have
14 lower mean values by including observations to the south. This causes the stratospheric
15 column from the TEMPO algorithm to be systematically biased high compared to the global
16 algorithm, translating into an underestimate in the tropospheric column (by more than $-0.5 \times$
17 10^{15} molec cm^{-2} in some locations). By the same logic, there is a high bias (also more than
18 $+0.5 \times 10^{15}$ molec cm^{-2} on average) along the northern edge of the field of regard in July.
19 There are also small low biases in the tropospheric column throughout the eastern side of the
20 TEMPO field of regard over the Atlantic Ocean. By excluding more pristine ocean conditions
21 further to the east, the stratospheric column derived by the TEMPO algorithm is biased high
22 compared to the global algorithm, which again translates into an underestimate in the
23 tropospheric column.

24 In the absence of daily ancillary satellite data for estimating stratospheric NO_2 outside the
25 field of regard, a climatology built from satellite observations or model data could mitigate
26 these edge effects for near real time retrievals since the average latitudinal and seasonal
27 dependence of stratospheric NO_2 are generally well known. For example, tests conducted
28 using a monthly mean global stratospheric NO_2 estimate as the supporting data outside the
29 TEMPO field of regard improves the correlations in both cases ($R^2 = 0.999$ and slope = 1.010
30 for July and $R^2 = 0.999$ and slope = 1.002 for January), now with >99% of the monthly mean
31 pixels differing from the global algorithm results by less than 0.05×10^{15} molec cm^{-2} .



1 Similarly, we find weaker overall performance in the cases of partial fields of regard
2 without context from surrounding low Earth orbit observations. Figure 12 shows the July
3 mean tropospheric column retrievals calculated for 1130 UTC (east coast summer morning)
4 and the July mean tropospheric column retrievals for 0200 UTC (west coast summer
5 evening). Though this version of the algorithm performs less well compared to the results
6 from incorporating independent low Earth orbit observations, the spatial correlation is still
7 good ($R^2 = 0.944$, slope = 0.943 for 1130 UTC July; $R^2 = 0.964$, slope = 0.986 for 0200
8 UTC). The differences over most of the available domain remain small, with 90-95% of the
9 pixels having differences in the mean tropospheric column of less than $\pm 0.2 \times 10^{15}$ molec cm⁻²
10 compared to the global algorithm. Figure 13 shows the January mean tropospheric column
11 retrievals calculated for 1400 UTC (east coast winter morning) and the January mean
12 tropospheric column retrievals for 2300 UTC (west coast winter evening). The spatial
13 correlation in both cases remains strong, again with some systematic biases observed ($R^2 =$
14 0.996 , slope = 1.001 at 1400 UTC and $R^2 = 0.987$, slope = 1.019 at 2330 UTC). The biases
15 remain modest, with ~90% of the pixels being consistent to within 0.2×10^{15} cm⁻² of the
16 global implementation of the algorithm. Again, using a monthly climatology mitigates the
17 biases in all cases, with the smallest improvement for the retrieval in January at 1400 UTC
18 (going from 90% to 94% of the pixels being consistent to within 0.2×10^{15} cm⁻² of the global
19 implementation of the algorithm).

20

21 6 Conclusions

22 The TEMPO geostationary satellite instrument is expected to provide hourly observations
23 of NO₂ columns (among a variety of other measurements) over North America. Here, we have
24 developed and tested the first stratosphere-troposphere separation algorithm for TEMPO
25 geostationary satellite observations of atmospheric NO₂ column density. We use independent
26 measurements from a low Earth observing satellite instrument to identify likely locations of
27 tropospheric enhancements, and to provide context outside of the available TEMPO
28 measurements. We consider partial fields of regard as a function of time of day, and
29 implement a new filter based on stratospheric to tropospheric air mass factor ratios. We
30 investigate in particular the information penalty associated with the limited TEMPO fields of
31 regard as a function of season and time of day.



1 We find that our algorithm performs as well as a global low Earth orbit algorithm for
2 most scenarios. When the whole continent is observed, monthly mean agreement with
3 tropospheric NO₂ retrieved from the global algorithm is excellent ($R^2 = 0.999$, slope = 1.009
4 for July and $R^2 = 0.998$, slope = 0.999 January). During most instances with a partial field of
5 regard (e.g. east coast morning or west coast evening) the algorithm still performs robustly.
6 We demonstrate that small biases near the southern and northern edges of the field of regard
7 are avoided by incorporating independent low Earth orbit observations that have been
8 corrected for the time of day. When the whole continent is observed, the vast majority of
9 pixels (> 95%) agree with results from a global implementation of the same algorithm to
10 within $\pm 0.05 \times 10^{15}$ molecules cm⁻². We find that the TEMPO algorithm is challenged most
11 by winter east coast morning retrievals, but nonetheless the difference between the TEMPO
12 algorithm and the global implementation of the same algorithm produces differences that are
13 less than 0.2×10^{15} molecules cm⁻² for more than 90% of the pixels. Even when supporting
14 observations from low Earth orbit may not be available (as in near-real-time), a large majority
15 of pixels (~90% or greater) agree with the global algorithm to within $\pm 0.2 \times 10^{15}$ molecules
16 cm⁻² on a monthly mean basis, which is generally accepted as typical estimates of
17 stratospheric error due to stratosphere-troposphere separation algorithms. The differences can
18 be reduced further in near-real-time retrievals by the use of a climatology outside the TEMPO
19 field of regard. The value of independent low Earth orbit observations for TEMPO
20 tropospheric retrievals implies benefit to TEMPO data from ongoing development of low
21 Earth orbit observations.

22 We have demonstrated a feasible and robust stratosphere-troposphere separation
23 algorithm for the retrieval of geostationary satellite-based NO₂ tropospheric column densities
24 by the TEMPO instrument notwithstanding the limited field of regard or changing time of
25 day. This approach may be applicable to other planned geostationary satellite instruments
26 including Sentinel-4 over Europe and GEMS over Asia. This spatial filtering and
27 interpolation method may also have applications in offset removal during retrievals of HCHO
28 and SO₂ tropospheric columns.

29

30 **Acknowledgements**

31 The authors are grateful to Kelly Chance, Xiong Liu, John Houck, Peter Zoogman, other
32 members of the TEMPO trace gas retrieval team for their input in preparation of this



1 manuscript. Work at Dalhousie University was supported by Environment and Climate
2 Change Canada. The authors also gratefully acknowledge the free use of TEMIS NO₂ data
3 from the GOME-2 sensor provided by www.temis.nl, and the NASA Standard Product NO₂
4 data from OMI provided by [http://disc.sci.gsfc.nasa.gov/Aura/data-](http://disc.sci.gsfc.nasa.gov/Aura/data-holdings/OMI/omno2_v003.shtml)
5 [holdings/OMI/omno2_v003.shtml](http://disc.sci.gsfc.nasa.gov/Aura/data-holdings/OMI/omno2_v003.shtml).

6

7 References

8 Adams, C., Normand, E. N., McLinden, C. A., Bourassa, A. E., Lloyd, N. D., Degenstein, D.
9 A., Krotkov, N. A., Belmonte Rivas, M., Folkert Boersma, K. and Eskes, H.: Limb-nadir
10 matching using non-coincident NO₂ observations: Proof of concept and the OMI-minus-
11 OSIRIS prototype product, *Atmos. Meas. Tech.*, 9(8), 4103–4122, doi:10.5194/amt-9-4103-
12 2016, 2016.

13 Bechle, M. J., Millet, D. B. and Marshall, J. D.: Remote sensing of exposure to NO₂: Satellite
14 versus ground-based measurement in a large urban area, *Atmos. Environ.*, 69, 345–353,
15 doi:10.1016/j.atmosenv.2012.11.046, 2013.

16 Beirle, S., Platt, U., Wenig, M. and Wagner, T.: Weekly cycle of NO₂ by GOME
17 measurements: a signature of anthropogenic sources, *Atmos. Chem. Phys.*, 3, 2225–2232,
18 2003.

19 Beirle, S., Kühl, S., Puķīte, J. and Wagner, T.: Retrieval of tropospheric column densities of
20 NO₂ from combined SCIAMACHY nadir/limb measurements, *Atmos. Meas. Tech.*, 3(1),
21 283–299, doi:10.5194/amt-3-283-2010, 2010.

22 Beirle, S., Hörmann, C., Jöckel, P., Liu, S., Penning de Vries, M., Pozzer, A., Sihler, H.,
23 Valks, P. and Wagner, T.: The STRatospheric Estimation Algorithm from Mainz (STREAM):
24 estimating stratospheric NO₂ from nadir-viewing satellites by weighted convolution, *Atmos.*
25 *Meas. Tech.*, 9(7), 2753–2779, doi:10.5194/amt-9-2753-2016, 2016.

26 Bobbink, R., Hicks, K., Galloway, J., Spranger, T., Alkemade, R., Ashmore, M., Bustamante,
27 M., Cinderby, S., Davidson, E., Dentener, F., Emmett, B., Erisman, J.-W., Fenn, M., Gilliam,
28 F., Nordin, A., Pardo, L. and De Vries, W.: Global assessment of nitrogen deposition effects
29 on terrestrial plant diversity: a synthesis, *Ecol. Appl.*, 20(1), 30–59, doi:10.1890/08-1140.1,
30 2010.



- 1 Boersma, K. F., Eskes, H. J. and Brinksma, E. J.: Error analysis for tropospheric NO₂
2 retrieval from space, *J. Geophys. Res.*, 109(D4), D04311–D04311,
3 doi:10.1029/2003JD003962, 2004.
- 4 Boersma, K. F., Eskes, H. J., Veefkind, J. P., Brinksma, E. J., van der A, R. J., Sneep, M., van
5 den Oord, G. H. J., Levelt, P. F., Stammes, P., Gleason, J. F. and Bucsela, E. J.: Near-real
6 time retrieval of tropospheric NO₂ from OMI, *Atmos. Chem. Phys.*, 7(8), 2103–2118,
7 doi:10.5194/acp-7-2103-2007, 2007.
- 8 Boersma, K. F., Jacob, D. J., Trainic, M., Rudich, Y., DeSmedt, I., Dirksen, R., and Eskes, H.
9 J.: Validation of urban NO₂ concentrations and their diurnal and seasonal variations observed
10 from the SCIAMACHY and OMI sensors using in situ surface measurements in Israeli cities,
11 *Atmos. Chem. Phys.*, 9, 3867–3879, doi:10.5194/acp-9-3867-2009, 2009.
- 12 Bovensmann, H., Burrows, J. P., Buchwitz, M., Frerick, J., Noël, S., Rozanov, V. V., Chance,
13 K. V., Goede, A. P. H., Bovensmann, H., Burrows, J. P., Buchwitz, M., Frerick, J., Noël, S.,
14 Rozanov, V. V., Chance, K. V. and Goede, A. P. H.: SCIAMACHY: Mission Objectives and
15 Measurement Modes, *J. Atmos. Sci.*, 56(2), 127–150, doi:10.1175/1520-
16 0469(1999)056<0127:SMOAMM>2.0.CO;2, 1999.
- 17 Bucsela, E. J., Celarier, E. A., Wenig, M. O., Gleason, J. F., Veefkind, J. P., Boersma, K. F.
18 and Brinksma, E. J.: Algorithm for NO₂ vertical column retrieval from the ozone monitoring
19 instrument, *IEEE Trans. Geosci. Remote Sens.*, 44(5), 1245–1257, 2006.
- 20 Bucsela, E. J., Krotkov, N. A., Celarier, E. A., Lamsal, L. N., Swartz, W. H., Bhartia, P. K.,
21 Boersma, K. F., Veefkind, J. P., Gleason, J. F. and Pickering, K. E.: A new stratospheric and
22 tropospheric NO₂ retrieval algorithm for nadir-viewing satellite instruments: applications to
23 OMI, *Atmos. Meas. Tech.*, 6(10), 2607–2626, doi:10.5194/amt-6-2607-2013, 2013.
- 24 Dirksen, R. J., Boersma, K. F., Eskes, H. J., Ionov, D. V., Bucsela, E. J., Levelt, P. F. and
25 Kelder, H. M.: Evaluation of stratospheric NO₂ retrieved from the Ozone Monitoring
26 Instrument: Intercomparison, diurnal cycle, and trending, *J. Geophys. Res.*, 116(D8), D08305,
27 doi:10.1029/2010JD014943, 2011.
- 28 Duncan, B. N., Yoshida, Y., de Foy, B., Lamsal, L. N., Streets, D. G., Lu, Z., Pickering, K. E.
29 and Krotkov, N. A.: The observed response of Ozone Monitoring Instrument (OMI) NO₂
30 columns to NO_x emission controls on power plants in the United States: 2005–2011, *Atmos.*
31 *Environ.*, 81, 102–111, doi:10.1016/j.atmosenv.2013.08.068, 2013.



- 1 Finlayson-Pitts, B. and Pitts, J.: Chemistry of the Upper and Lower Atmosphere. Theory,
2 Experiments, and Applications, Academic Press, 1999.
- 3 Geddes, J. A. and Martin, R. V.: Global deposition of total reactive nitrogen oxides from 1996
4 to 2014 constrained with satellite observations of NO₂ columns, Atmos. Chem. Phys.
5 Discuss., 1–44, doi:10.5194/acp-2016-1100, 2017.
- 6 Geddes, J. A., Martin, R. V., Boys, B. L. and van Donkelaar, A.: Long-Term Trends
7 Worldwide in Ambient NO₂ Concentrations Inferred from Satellite Observations, Environ.
8 Health Perspect., Advance Pu, doi:10.1289/ehp.1409567, 2016.
- 9 Hilboll, A., Richter, A., Rozanov, A., Hodnebrog, Heckel, A., Solberg, S., Stordal, F. and
10 Burrows, J. P.: Improvements to the retrieval of tropospheric NO₂ from satellite -
11 Stratospheric correction using SCIAMACHY limb/nadir matching and comparison to Oslo
12 CTM2 simulations, Atmos. Meas. Tech., 6(3), 565–584, doi:10.5194/amt-6-565-2013, 2013.
- 13 Ialongo, I., J. Hermann, N. Krotkov, L. Lamsal, K. F. Boersma, J. Hovila, and J. Tamminen,
14 Comparison of OMI NO₂ observations and their seasonal and weekly cycles with ground-
15 based measurements in Helsinki, Atmos. Meas. Tech., 9, 5203-5212, doi: 10.5194/amt-9-
16 5203-2016, 2016.
- 17 Jaegle, L., Steinberger, L., Martin, R. V and Chance, K.: Global partitioning of NO_x sources
18 using satellite observations: Relative roles of fossil fuel combustion, biomass burning and soil
19 emissions, Faraday Discuss., 130, 407–423, doi:10.1039/b502128f, 2005.
- 20 Jia, Y., Yu, G., Gao, Y., He, N., Wang, Q., Jiao, C. and Zuo, Y.: Global inorganic nitrogen
21 dry deposition inferred from ground- and space-based measurements., Sci. Rep., 6, 19810,
22 doi:10.1038/srep19810, 2016.
- 23 Konovalov, I. B., Beekmann, M., Burrows, J. P. and Richter, A.: Satellite measurement based
24 estimates of decadal changes in European nitrogen oxides emissions, Atmos. Chem. Phys.,
25 8(10), 2623–2641, doi:10.5194/acp-8-2623-2008, 2008.
- 26 Krotkov, N. A., Lamsal, L. N., Celarier E. A., Swartz, W. H., Marchenko, S. V., Bucsela, E.
27 J., Chan, K. L., Wenig, M., Zara, M.: The version 3 OMI NO₂ standard product, Atmos.
28 Meas. Tech., 10, 3133-3149, <https://doi.org/10.5194/amt-10-3133-2017>, 2017.
- 29 Lamsal, L. N., Martin, R. V., van Donkelaar, A., Steinbacher, M., Celarier, E. A., Bucsela, E.,
30 Dunlea, E. J., Pinto, J. P.: Ground-level nitrogen dioxide concentrations inferred from the



- 1 satellite-borne Ozone Monitoring Instrument, *J. Geophys. Res.-Atm.*, 113, D16308,
2 doi:10.1029/2007JD009235, 2008.
- 3 Lamsal, L. N., Martin, R. V., Padmanabhan, A., Van Donkelaar, A., Zhang, Q., Sioris, C. E.,
4 Chance, K., Kurosu, T. P. and Newchurch, M. J.: Application of satellite observations for
5 timely updates to global anthropogenic NO_x emission inventories, *Geophys. Res. Lett.*, 38(5),
6 2011.
- 7 Lamsal, L. N., Krotkov, N. A., Celarier, E. A., Swartz, W. H., Pickering, K. E., Bucsela, E. J.,
8 Gleason, J. F., Martin, R. V., Philip, S., Irie, H., Cede, A., Herman, J., Weinheimer, A.,
9 Szykman, J. J., and Knepp, T. N.: Evaluation of OMI operational standard NO₂ column
10 retrievals using in situ and surface-based NO₂ observations, *Atmos. Chem. Phys.*, 14, 11587–
11 11609, doi:10.5194/acp-14-11587-2014, 2014.
- 12 Lasnik J, Stephens M, Baker B, Randall C, Ko DH, Kim S, et al. 2014. Geostationary
13 Environment Monitoring Spectrometer (GEMS) over the Korea peninsula and Asia-Pacific
14 region. Abstract A51A-3003 presented at 2014 Fall Meeting, AGU, 15–19 December 2014,
15 San Francisco, California.
- 16 Leue, C., Wenig, M., Wagner, T., Klimm, O., Platt, U. and Jähne, B.: Quantitative analysis of
17 NO_x emissions from Global Ozone Monitoring Experiment satellite image sequences, *J.*
18 *Geophys. Res. Atmos.*, 106(D6), 5493–5505, doi:10.1029/2000JD900572, 2001.
- 19 Martin, R. V.: Global inventory of nitrogen oxide emissions constrained by space-based
20 observations of NO₂ columns, *J. Geophys. Res.*, 108(D17), 4537,
21 doi:10.1029/2003JD003453, 2003.
- 22 Martin, R. V., Chance, K., Jacob, D. J., Kurosu, T. P., Spurr, R. J. D., Bucsela, E., Gleason, J.
23 F., Palmer, P. I., Bey, I., Fiore, A. M., Li, Q., Yantosca, R. M. and Koelemeijer, R. B. A.: An
24 improved retrieval of tropospheric nitrogen dioxide from GOME, *J. Geophys. Res.*,
25 107(D20), 4437, doi:10.1029/2001JD001027, 2002.
- 26 McLinden, C. A., Fioletov, V., Boersma, K. F., Krotkov, N., Sioris, C. E., Veefkind, J. P. and
27 Yang, K.: Air quality over the Canadian oil sands: A first assessment using satellite
28 observations, *Geophys. Res. Lett.*, 39(4), n/a-n/a, doi:10.1029/2011GL050273, 2012.
- 29 Miyazaki, K., Eskes, H., Sudo, K., Boersma, K. F., Bowman, K. and Kanaya, Y.: Decadal
30 changes in global surface NO_x emissions from multi-constituent satellite data assimilation,
31 *Atmos. Chem. Phys. Discuss.*, 1–48, doi:10.5194/acp-2016-529, 2016.



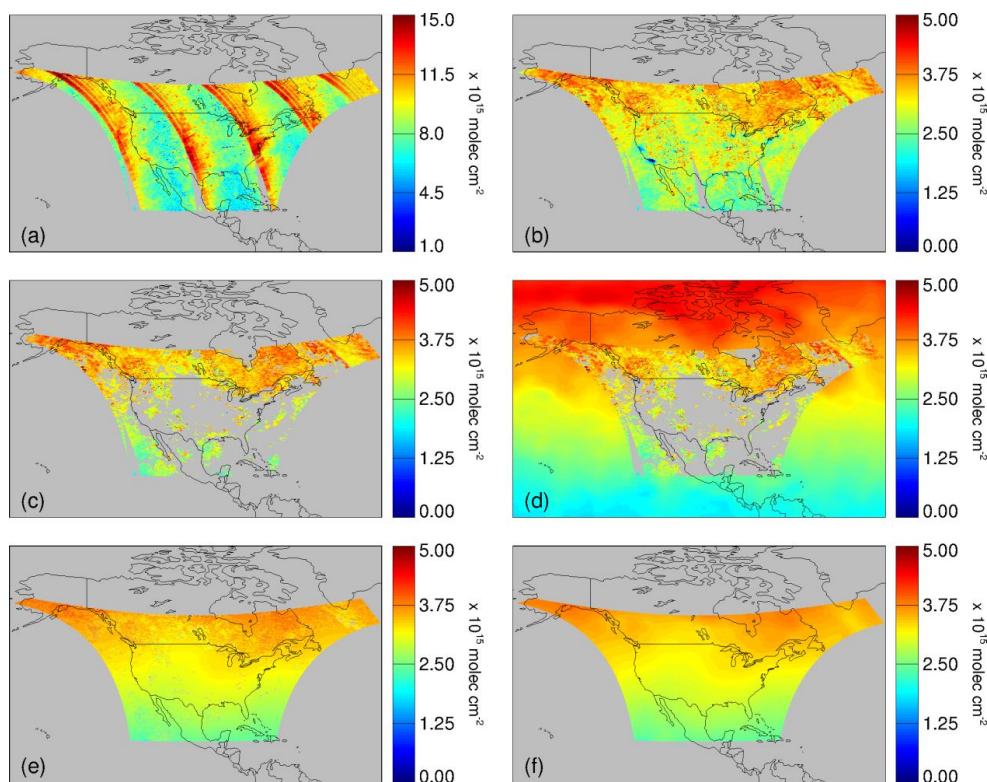
- 1 Nowlan, C. R., Martin, R. V., Philip, S., Lamsal, L. N., Krotkov, N. A., Marais, E. A., Wang,
2 S. and Zhang, Q.: Global dry deposition of nitrogen dioxide and sulfur dioxide inferred from
3 space-based measurements, *Global Biogeochem. Cycles*, n/a-n/a,
4 doi:10.1002/2014GB004805, 2014.
- 5 Richter, A. and Burrows, J. P.: Tropospheric NO₂ from GOME measurements, *Adv. Sp. Res.*,
6 29(11), 1673–1683, doi:10.1016/S0273-1177(02)00100-X, 2002.
- 7 Richter, A., Burrows, J. P., Nüss, H., Granier, C. and Niemeier, U.: Increase in tropospheric
8 nitrogen dioxide over China observed from space., *Nature*, 437(7055), 129–32,
9 doi:10.1038/nature04092, 2005.
- 10 Russell, A. R., Valin, L. C. and Cohen, R. C.: Trends in OMI NO₂ observations over the
11 United States: effects of emission control technology and the economic recession, *Atmos.*
12 *Chem. Phys.*, 12(24), 12197–12209, doi:10.5194/acp-12-12197-2012, 2012.
- 13 Seinfeld, J. H. and Pandis, S. N.: *Atmospheric Chemistry and Physics: from air pollution to*
14 *climate change*, 3rd ed., John Wiley & Sons Inc., Hoboken New Jersey., 2016.
- 15 Sussmann, R., Stremme, W., Burrows, J. P., Richter, A., Seiler, W. and Rettinger, M.:
16 Stratospheric and tropospheric NO₂ variability on the diurnal and annual scale: a combined
17 retrieval from ENVISAT/SCIAMACHY and solar FTIR at the Permanent Ground-Truthing
18 Facility Zugspitze/Garmisch, *Atmos. Chem. Phys.*, 5(10), 2657–2677, doi:10.5194/acp-5-
19 2657-2005, 2005.
- 20 Valks, P., Pinardi, G., Richter, A., Lambert, J.-C., Hao, N., Loyola, D., Van Roozendaal, M.
21 and Emmadi, S.: Operational total and tropospheric NO₂ column retrieval for GOME-2,
22 *Atmos. Meas. Tech.*, 4(7), 1491–1514, doi:10.5194/amt-4-1491-2011, 2011.
- 23 Velders, G. J. M., Granier, C., Portmann, R. W., Pfeilsticker, K., Wenig, M., Wagner, T.,
24 Platt, U., Richter, A. and Burrows, J. P.: Global tropospheric NO₂ column distributions:
25 Comparing three-dimensional model calculations with GOME measurements, *J. Geophys.*
26 *Res. Atmos.*, 106(D12), 12643–12660, doi:10.1029/2000JD900762, 2001.
- 27 Veihelmann B, Meijer Y, Ingmann P, Koopman R, Wright N, Bazalgette Courrèges-Lacoste
28 G, et al. The Sentinel-4 mission and its atmospheric composition products. In: Proceedings of
29 the 2015 EUMETSAT meteorological satellite conference. France, 21–25 September 2015.
- 30 Wenig, M., Köhl, S., Beirle, S., Bucsela, E., Jähne, B., Platt, U., Gleason, J. and Wagner, T.:



- 1 Retrieval and analysis of stratospheric NO₂ from the Global Ozone Monitoring Experiment,
- 2 J. Geophys. Res. Atmos., 109(D4), n/a-n/a, doi:10.1029/2003JD003652, 2004.
- 3 Zoogman, P., Liu, X., Suleiman, R. M., Pennington, W. F., Flittner, D. E., Al-Saadi, J. A.,
- 4 Hilton, B. B., Nicks, D. K., Newchurch, M. J., Carr, J. L., Janz, S. J., Andraschko, M. R.,
- 5 Arola, A., Baker, B. D., Canova, B. P., Chan Miller, C., Cohen, R. C., Davis, J. E., Dussault,
- 6 M. E., Edwards, D. P., Fishman, J., Ghulam, A., González Abad, G., Grutter, M., Herman, J.
- 7 R., Houck, J., Jacob, D. J., Joiner, J., Kerridge, B. J., Kim, J., Krotkov, N. A., Lamsal, L., Li,
- 8 C., Lindfors, A., Martin, R. V., McElroy, C. T., McLinden, C., Natraj, V., Neil, D. O.,
- 9 Nowlan, C. R., O'Sullivan, E. J., Palmer, P. I., Pierce, R. B., Pippin, M. R., Saiz-Lopez, A.,
- 10 Spurr, R. J. D., Szykman, J. J., Torres, O., Veefkind, J. P., Veihelmann, B., Wang, H., Wang,
- 11 J. and Chance, K.: Tropospheric emissions: Monitoring of pollution (TEMPO), J. Quant.
- 12 Spectrosc. Radiat. Transf., 186, 17–39, doi:10.1016/j.jqsrt.2016.05.008, 2017.

13

14



1

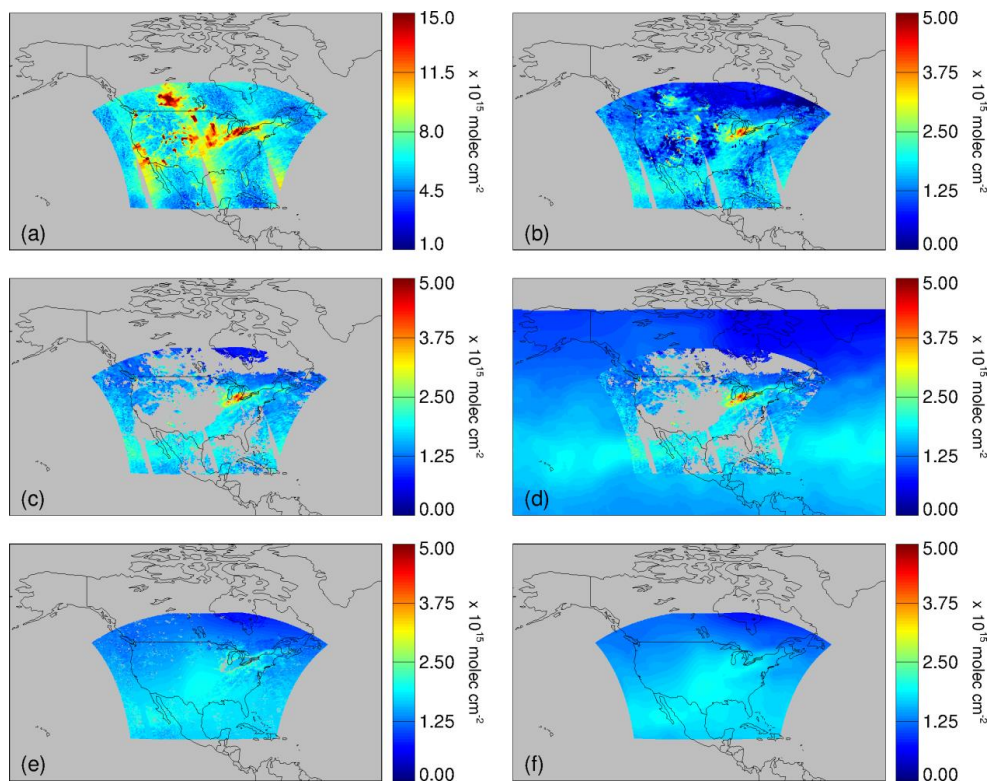
2 **Figure 1:** Calculation of the stratospheric NO₂ estimate on July 15, 2007 using OMI
3 observations from within the anticipated TEMPO field of regard: (a) Slant columns on a 0.1°
4 $\times 0.1^\circ$ grid. (b) Initial stratospheric estimate (V_{init}) resulting from Equation 1 and 2. (c)
5 Masked V_{init} using a threshold of $S_{trop}/A_{strat} < 0.3 \times 10^{15}$ molec cm⁻² to remove large
6 tropospheric influence. (d) Adding context outside of the TEMPO field of regard by using
7 independent low-earth orbit observations from GOME-2 that have been corrected for time of
8 day. (e) Stratospheric NO₂ estimate with masked areas interpolated. (f) Stratospheric NO₂
9 estimate after final hot spot removal and smoothing.

10

11



1
2



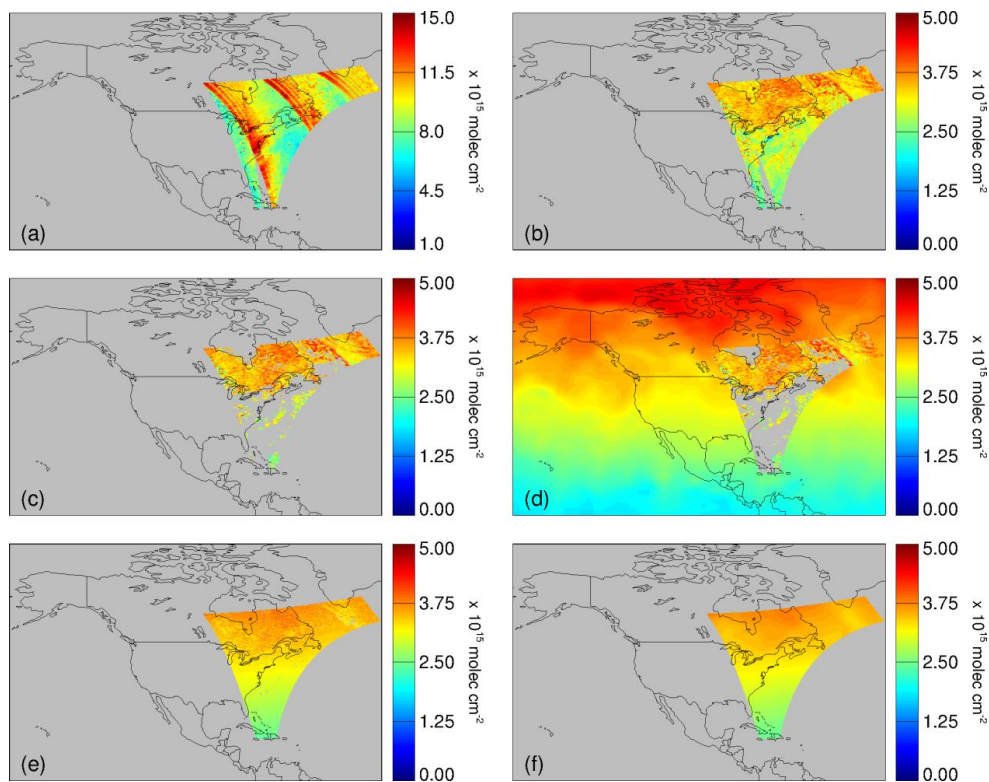
3

4 **Figure 2:** Calculation of the stratospheric NO₂ estimate on January 15, 2007 using OMI
5 observations from within the anticipated TEMPO field of regard: (a) Slant columns on a 0.1°
6 x 0.1° grid. (b) Initial stratospheric estimate (V_{init}) resulting from Equation 1 and 2. (c)
7 Masked V_{init} using a threshold of $S_{trop}/A_{strat} < 0.3 \times 10^{15} \text{ molec cm}^{-2}$ to remove large
8 tropospheric influence. (d) Adding context outside of the TEMPO field of regard by using
9 independent low-earth orbit observations from GOME-2 that have been corrected for time of
10 day. (e) Stratospheric NO₂ estimate with masked areas interpolated. (f) Stratospheric NO₂
11 estimate after final hot spot removal and smoothing.

12



1



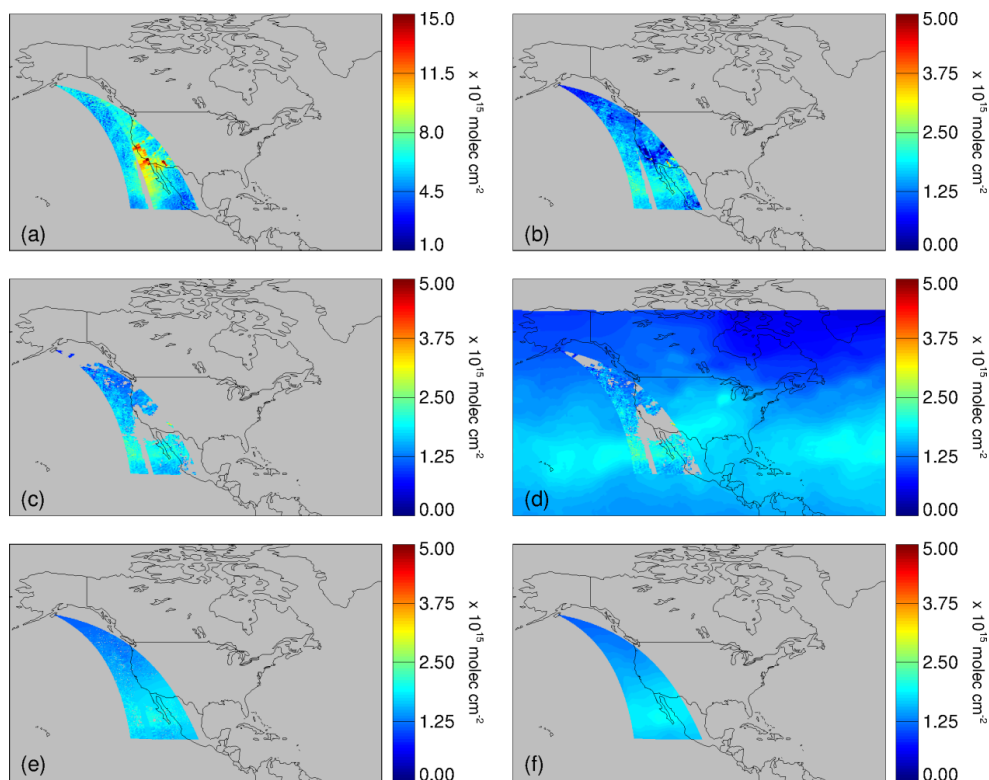
2

3 **Figure 3:** Calculation of the stratospheric NO₂ estimate on July 15, 2007 using OMI
4 observations from within the anticipated TEMPO field of regard at 1130 UTC (6:30 am
5 Eastern Standard Time): (a) Slant columns on a 0.1° x 0.1° grid. (b) Initial stratospheric
6 estimate (V_{init}) resulting from Equation 1 and 2. (c) Masked V_{init} using a threshold of S_{trop}/A_{strat}
7 $< 0.3 \times 10^{15}$ molec cm⁻² to remove large tropospheric influence. (d) Adding context outside of
8 the TEMPO field of regard by using independent low-earth orbit observations from GOME-2
9 that have been corrected for time of day. (e) Stratospheric NO₂ estimate with masked areas
10 interpolated and smoothed. (f) Stratospheric NO₂ estimate after final hot spot removal
11 smoothing.

12



1



2

3 **Figure 4:** Calculation of the stratospheric NO₂ estimate on January 15, 2007 using OMI
4 observations from within the anticipated TEMPO field of regard at 2330 UTC (3:30 pm
5 Pacific Standard Time): (a) Slant columns at 0.1° x 0.1° resolution. (b) Initial stratospheric
6 estimate (V_{init}) resulting from Equation 2. (c) Masked V_{init} using a threshold of $S_{trop}/A_{strat} < 0.3$
7 $\times 10^{15}$ molec cm⁻² to remove large tropospheric influence. (d) Adding context outside of the
8 available TEMPO field of regard by using independent low-earth orbit observations from
9 GOME-2 that have been corrected for time of day. (e) Stratospheric NO₂ estimate with
10 masked areas interpolated and smoothed. (f) Final stratospheric NO₂ estimate after hot spot
11 removal and smoothing.

12



1

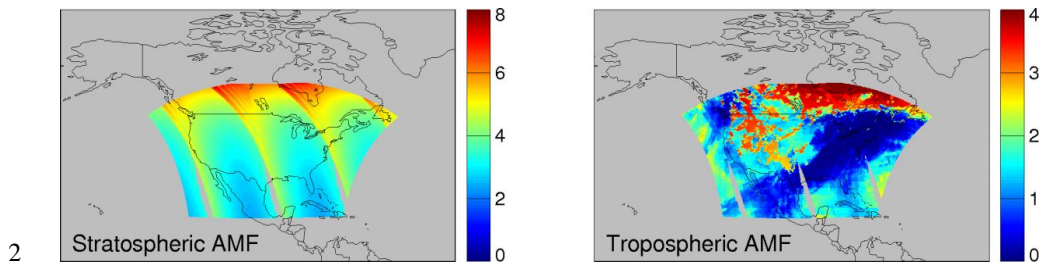
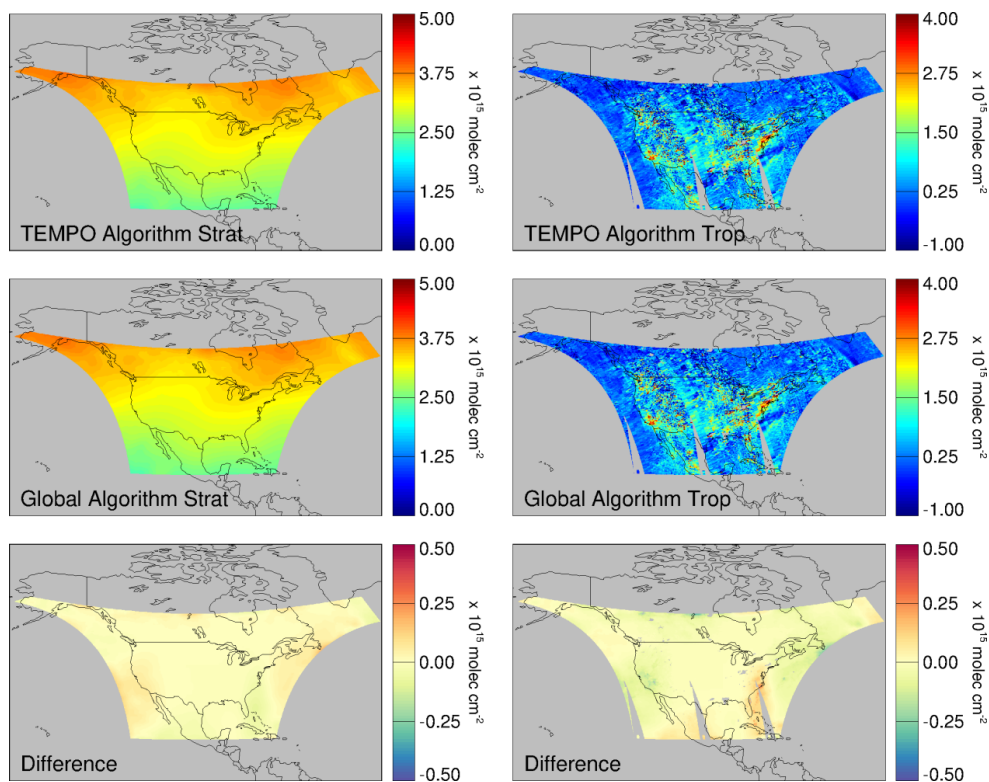


Figure 5: Stratospheric (left) and tropospheric (right) air mass factors for January 15, 2007.



1



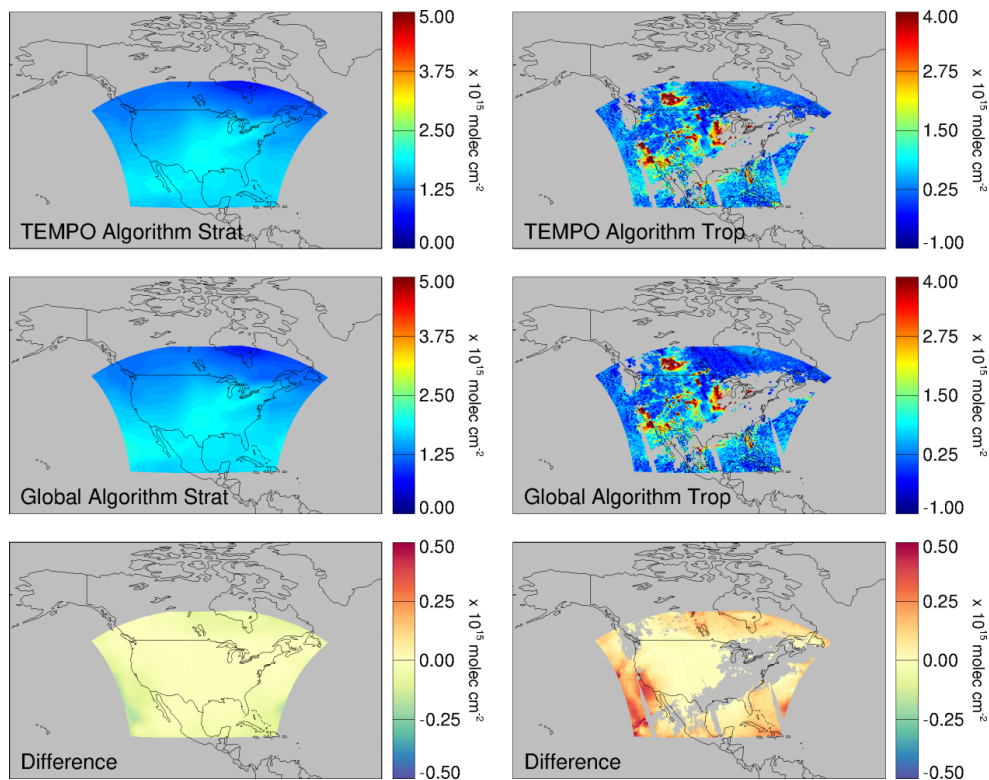
2

3 **Figure 6:** Stratospheric NO₂ (left panels) and final tropospheric NO₂ retrievals (right panels)
4 resulting from our stratosphere-troposphere separation algorithms for July 15, 2007. Top
5 panels show the results using our proposed TEMPO algorithm. Middle panels show the
6 results using global observations (results have been clipped to the TEMPO field of regard for
7 comparison). Bottom panels show the absolute absolute differences between the TEMPO
8 and global algorithm results.

9



1



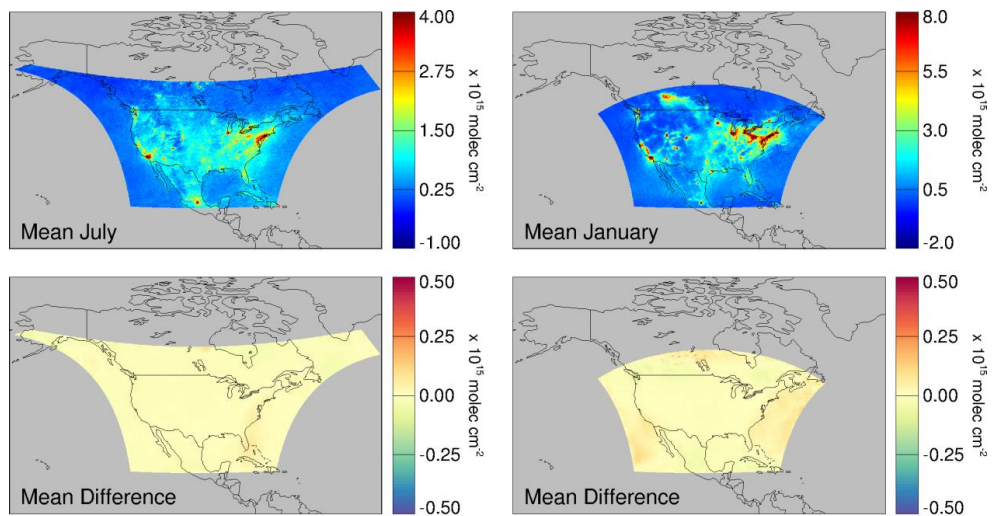
2

3 **Figure 7:** Stratospheric NO₂ (left panels) and final tropospheric NO₂ retrievals (right panels)
 4 resulting from our algorithm for January 15, 2007. Top panels show the results using our
 5 proposed TEMPO algorithm. Middle panels show the results using global observations
 6 (results have been clipped to the TEMPO field of regard for comparison). Bottom panels
 7 show the absolute differences between the TEMPO and global algorithm results.

8



1



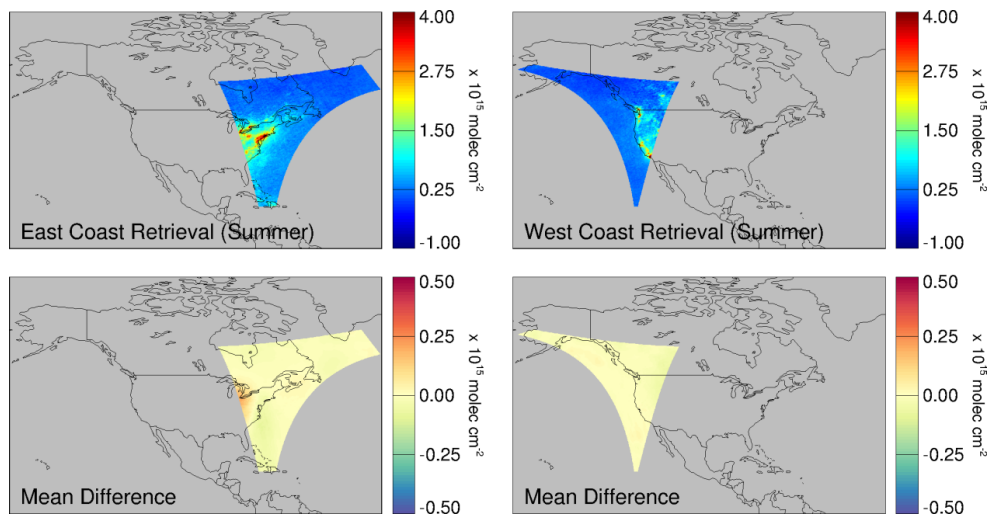
2

3 **Figure 8:** Top panels show mean July and January tropospheric NO₂ column densities
4 resulting from our TEMPO algorithm. Bottom panels show absolute difference in mean July
5 and January tropospheric NO₂ between the TEMPO algorithm and the global algorithm.

6



1



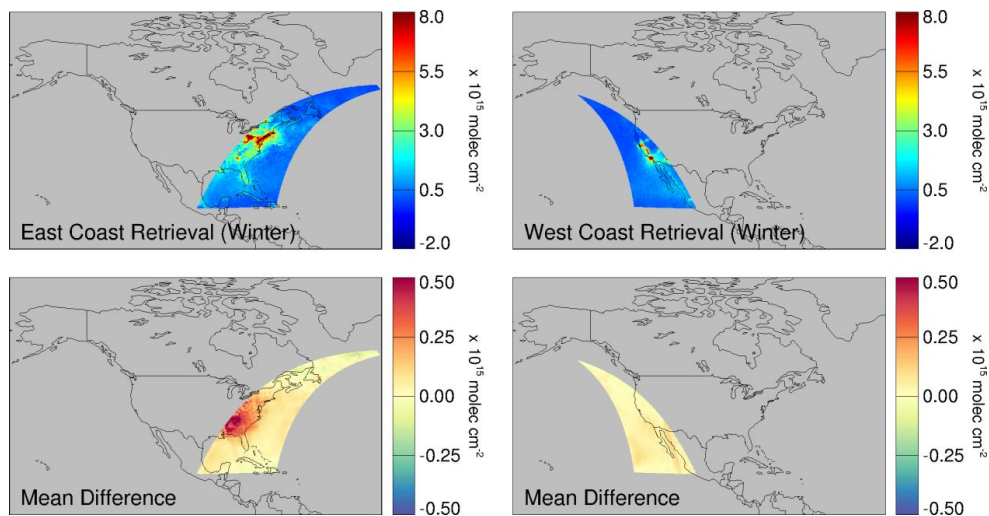
2

3 **Figure 9:** Top panels show mean July tropospheric NO₂ column densities at 1130 UTC (left)
 4 and 0200 UTC (right) resulting from our TEMPO STS algorithm. Bottom panels show
 5 absolute difference in the tropospheric NO₂ column between the TEMPO algorithm and the
 6 global STS algorithm.

7



1



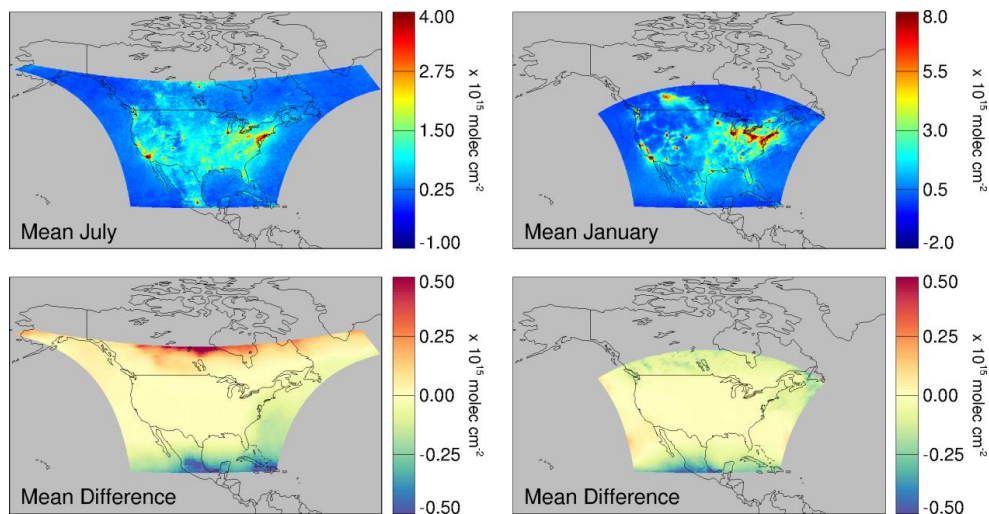
2

3 **Figure 10:** Top panels show mean January tropospheric NO₂ column densities at 1400 UTC
 4 (left) and 2330 UTC (right) resulting from our TEMPO STS algorithm. Middle panels show
 5 absolute difference in the tropospheric NO₂ column between the TEMPO algorithm and the
 6 global STS algorithm.

7



1



2

3 **Figure 11:** Top panels show mean July and January tropospheric NO₂ column densities
 4 resulting from our TEMPO STS algorithm without using independent low-earth orbit
 5 observations for context outside the TEMPO field of regard (as might be occasionally
 6 expected in near-real-time operations). Bottom panels show absolute difference in mean July
 7 and January tropospheric NO₂ between the TEMPO algorithm and the global STS algorithm.

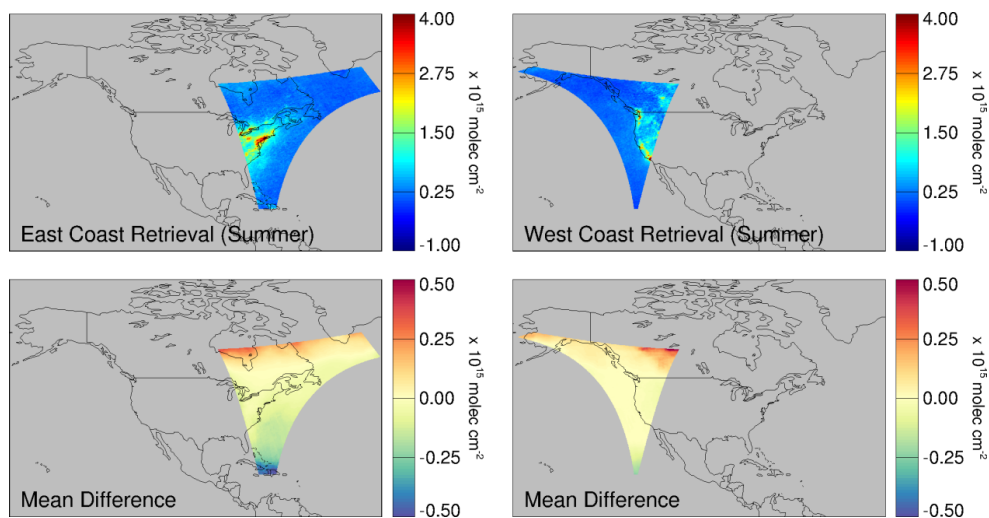
8

9



1

2



3

4 **Figure 12:** Top panels show mean July tropospheric NO₂ column densities at 1130 UTC (left)

5 and 0200 UTC (right) resulting from our TEMPO STS algorithm without using independent

6 low-earth orbit observations for context outside the TEMPO field of regard. Bottom panels

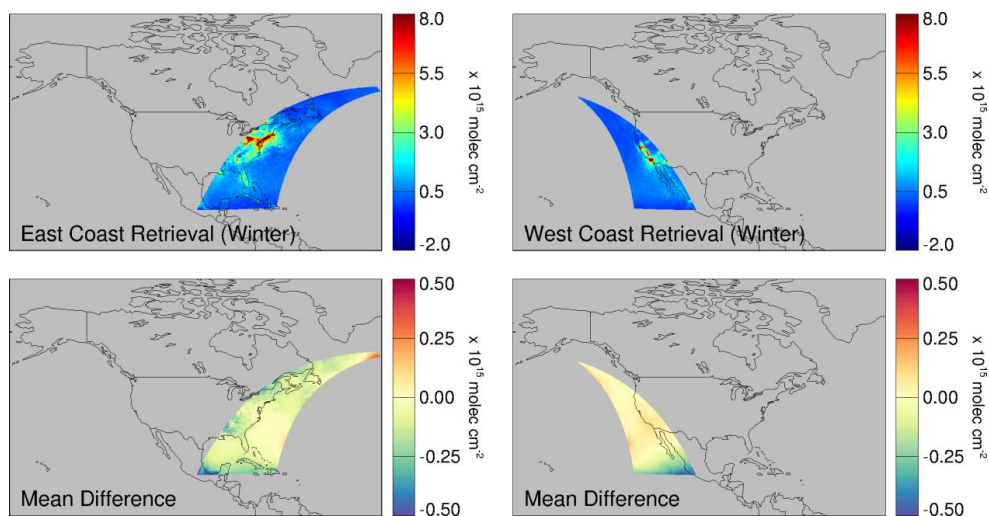
7 show absolute difference in the tropospheric NO₂ column between the TEMPO algorithm and

8 the global STS algorithm.

9



1



2

3 **Figure 13:** Top panels show mean January tropospheric NO₂ column densities at 1400 UTC
 4 (left) and 2330 UTC (right) resulting from our TEMPO algorithm without using independent
 5 low-earth orbit observations for context outside the TEMPO field of regard. Middle panels
 6 show absolute difference in the tropospheric NO₂ column between the TEMPO algorithm and
 7 the global algorithm.

8

9

10